ACS OMEGA

Open Access

http://pubs.acs.org/journal/acsodf

Article

Research on Flow Patterns of Two-Phase Fracturing Fluid in Hydraulic Fracture Considering the Fluid Leak-off

Yusong Chen,* Jingwei Li, Qi Song, Chengzhong Bu, Kairui Ye, Feng He, Zhuolun Lv, and Xiang Chen

Cite This: *ACS Omega* 2024, 9, 2432−2442

Read Online

ACCESS | Metrics & More | Article Recommendations

ABSTRACT: In in situ-generated proppant fracturing technology without proppant injection, the distribution of the flow pattern of two-phase fracturing fluid in the fracture determines the concentration of proppant particles formed by phase change in different positions. Therefore, the study of a two-phase fracturing fluid flow pattern is of great significance to reveal the formation mechanisms of different flow patterns and guide the on-site implementation of the technology. This paper establishes a mathematical model for the two-phase fracturing fluids in fractures based on their physical properties and presents numerical experiments on the flow pattern of two-phase fracturing fluids under different conditions of injection displacement, interfacial tension, and phase change liquid (PCL) ratio. The results show that at lower injection displacements, such as 3 or 4 m^3/min, it is easier to form striped shape distributions, and at higher injection displacements, such as 5 or 6 m^3/min, it is easier to form droplet shape distributions. When the interfacial tension is low (15 mN/m), PCL shrinks less and is distributed in strips; when the interfacial tension is high (25, 35, and 45 mN/m), PCL shrinks more and mainly forms droplet-shaped distributions. PCL tends to form discrete droplet shape distributions at PCL volume fractions of 10, and 20%. At 30% volume fraction, PCL is distributed in strips, and at 40% volume fraction, PCL forms strips of a larger size. These findings reveal the changing pattern of two-phase fracturing fluid flow and enrich the theoretical system of in situ-generated proppant fracturing technology, which can provide theoretical support for the on-site implementation of this technology.

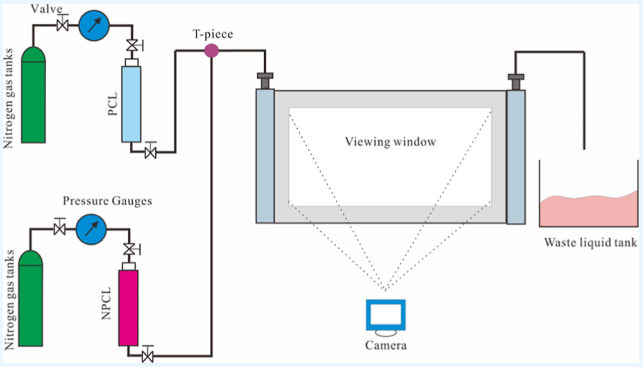

1. INTRODUCTION

In situ-generated proppant fracturing technology (Figure 1) was created to solve the issues of equipment wear by proppant, limited migration distance of proppant, and difficulties in supporting narrow fractures in conventional hydraulic fracturing technology.[1−3] It utilizes an immiscible two-phase fracturing fluid for work. One phase, known as phase change liquid (PCL), undergoes a phase transition and transforms into solid proppant particles when stimulated by the formation temperature. The other phase (NPCL, nonphase change liquid) occupies part of the fracture space, and the space liberated by its backflow functions as an oil and gas high-conductivity flow channel.[4,5] Due to the different physical properties, such as density and viscosity, of PCL and NPCL, as well as the existence of interfacial tension between the two immiscible fluids, they will flow in fractures in different ways. The distribution of the flow pattern is determined by the concentration of proppant particles at different positions in the fracture after the phase transition, which affects the support effect and conductivity. Therefore, studying the flow patterns of the two-phase fracturing fluid is of great significance for revealing the formation mechanisms of different flow patterns and guiding the on-site implementation of in situ-generated proppant fracturing technology. As shown in Figure 1, PFFS means the phase-transition fracturing fluid system; it is the mixture of PCL and NPCL; IGP means in situ-generated proppant; it is the proppant particles formed by phase change from PCL.

The flow pattern of two-phase fracturing fluid belongs to the field of liquid−liquid two-phase flow,[6] the PCL and the NPCL were injected, both of which are immiscible, from the inlet, and the boundary condition was set at the inlet as a velocity inlet and the outlet as a pressure outlet. Formation rock is a kind of porous medium. A part of the PCL and NPCL in the hydraulic fracture will leak off into the formation along the direction perpendicular to the wall of the hydraulic fracture, resulting in the total volume of PFFS in hydraulic fractures being less than the volume injected.

Received: September 9, 2023
Revised: November 25, 2023
Accepted: November 30, 2023
Published: January 1, 2024

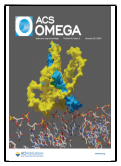

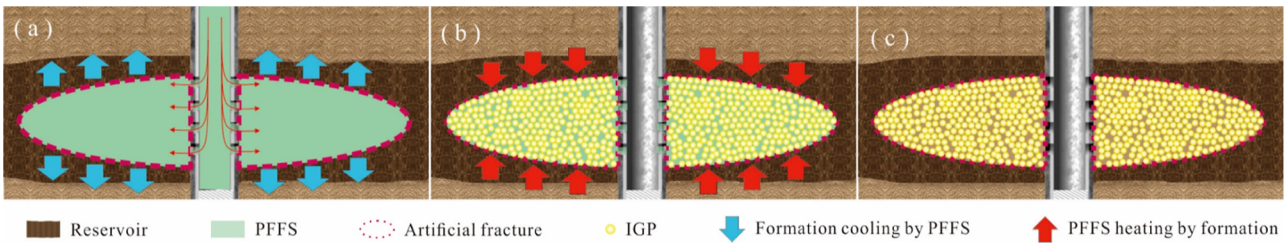

Figure 1. Principle of in situ-generated proppant fracturing technology: (a) continuous injection PFFS cooling the formation, (b) formation heating the injected PFFS and IGP formed by the thermal stimulation, and (c) NPCL flow back and IGP remaining in the fracture and prop the hydraulic fracture.

The relevant research mainly focuses on experimental research and flow pattern discrimination. In terms of experimental research, research methods include physical and numerical experiments. Due to the advantages of numerical experimental research in terms of time investment, economic cost, and experimental conditions, it has received increasing attention. Zhang et al.[7] carried out a numerical study on the two-phase flow problem in oil−water separators, and flow characteristics such as pressure drop, cross-sectional phase distribution, and outlet flow rate were obtained. The effects of geometric parameters such as conical angle, pipe diameter, pitch height, and outlet split ratio on oil−water separation are revealed. Archibong-Eso et al.[8] carried out a numerical simulation of a two-phase flow of high-viscosity oil and water in a pipeline using commercial software with oil viscosities between 3.5 and 5 Pa.s. The apparent flow velocities of oil and water in the experiments ranged from 0.06 to 0.55 m/s and from 0.01 to 1.0 m/s. The above studies are all focused on the two-phase flow pattern in pipelines with circular cross sections. For flow channels with rectangular cross sections, the flow pattern may vary slightly. In response, Abdul Hussein et al.[9] carried out a numerical experimental analysis on the effect of geometry on two-phase flow patterns using the volume of fluid (VOF) and mixed multiphase flow modeling methods in conjunction with a normal k-ε turbulence scheme. Song et al.[10] conducted visualization experiments on water flooding in fractures to analyze the effects of factors such as gravity differentiation, water injection velocity, displacement direction, and fracture opening on the morphology of oil−water flow and oil displacement effectiveness. Babaoğlu et al.[11] have explored the effect of cross-sectional shape (circular, elliptical, rectangular, square, and trapezoidal) on flow patterns and pressure drop.

In terms of flow pattern discrimination, Sarkar et al.[12] classified liquid−liquid two-phase flow patterns in serpentine glass microchannels into segmental plug flow, segmental plug and droplet flow, droplet flow, unsteady annular flow, annular flow, annular dispersed flow, and fully dispersed flow and presented Voronoi diagrams of the flow regime maps. Mao et al.[13] studied the morphology of oil−water two-phase flow in batch transportation of oil and water and found that the oil−water interface is more stable than the oil−water interface. The oil−water flow pattern is divided into annular flow, stratified flow, dispersed flow, and transitional flow between annular flow and dispersed flow. The initial oil body integral number and flow rate are key factors that control the total length of the oil continuous section. Tan et al.[14] investigated the impact of pipeline diameter and viscosity on flow patterns, classifying low-viscosity oil and water flow patterns in large-diameter pipelines as stratified flow, scattered flow, and transitional flow. High-viscosity oil and water flows have annular flows in addition to these other flows. Low-viscosity and high-viscosity oil and water flow features stratified flow, scattered flow, annular flow, and intermittent flow patterns in small-diameter pipes. Wang et al.[15] investigated the flow patterns of acid and fracturing fluids in acid fracturing, looking at how viscosity, injection rate, and alternate injection sequence affected the flow distribution pattern of acid and fracturing fluids. The existing models use FVM (finite volume method), VOF method, level set, and other methods to study the distribution of liquid−liquid two-phase flow patterns. However, for the two-phase fracturing fluid flow pattern studied in this paper, it is necessary to consider the leak-off of the fluid into the reservoir matrix. The existing model does not consider the effect of the leak-off on the flow pattern and cannot fully explain the formation mechanism of the two-phase fracturing fluid flow pattern in the hydraulic fracture.[16]

Currently, on the one hand, when two-phase fracturing fluid is injected into a hydraulic fracture, a large portion of it will be filtered out to the formation near the fracture,[17] resulting in a decrease in the volume of fracturing fluid inside the fracture.[18] The leak-off rate of PCL is much higher than that of NPCL,[19] leading to a significant change in the ratio of PCL to NPCL in the fractures. On the other hand, the physical properties of PCL and NPCL are greatly affected by temperature, and they exhibit different interfacial tensions under different temperature conditions.[20] Under the comprehensive influence of changes in the ratio of PCL to NPCL and interfacial tension, the flow pattern of the two-phase fracturing fluid undergoes significant changes. However, existing research on two-phase flow patterns is mainly conducted under fixed two-phase ratio and interface tension conditions, lacking research on flow patterns under changing two-phase ratio and interface tension conditions, and without considering the impact of filtration, it cannot fully reveal the formation mechanisms of different two-phase flow forms in situ-generated proppant fracturing technology, which limits further application of this technology.

In this regard, this paper combines the physical properties of two-phase fracturing fluid and the implementation plan of in situ-generated proppant fracturing technology to construct a mathematical model for the flow pattern distribution of two-phase fracturing fluid. Through mathematical models, the mechanism of injection displacement, interfacial tension, and the PCL ratio on the formation of a two-phase flow pattern is revealed, which provides theoretical support for the on-site implementation of in situ-generated proppant fracturing technology.

2. MATHEMATICAL MODEL OF FLOW PATTERNS

In this section, the two-phase fracturing fluid model is established based on the discretized virtual internal bonds (DVIB) method, the Navier−Stokes (N−S) equation is used to

https://doi.org/10.1021/acsomega.3c06877
ACS Omega 2024, 9, 2432−2442

establish a mathematical model of the fluid flow field in a fracture, and the VOF method is used to establish a mathematical model of the flow distribution of two-phase fracturing fluid in a fracture.

2.1. Flow Model of Two-Phase Fracturing Fluid Leak-off in the Formation. The leak-off depth and leak-off velocity of the fracturing fluid are important factors that influence the effect of fracturing.[21,22] Classical leak-off theory defines that it is controlled by three mechanisms: the viscosity of the fracturing fluid, the compressibility of the reservoir rock and fluid, and the wall-forming properties of the fracturing fluid.[23] The continuity equation for the in-seam fluid pressure drop is included in the in-seam flow pattern model developed in this paper, and the effect of the leak-off rate on the fluid pressure field is introduced.

The NPCL viscosity is lower than PCL and the leak-off is larger,[24] while the PCL viscosity is higher and the phase change in the fracture is faster, the leak-off is smaller, and the PCL leak-off tends to be stable after more than 20 min; the repulsion experiments also show that the volume of PCL flowing through the core under the repulsion pressure difference is very small, and most of the PCL is retained at the injection end; therefore, the effect of PCL leak-off velocity can be ignored, and only, the effect of PCL leak-off rate can be ignored, and only the effect of NPCL leak-off rate on the flow distribution pattern can be considered.

The DVIB method was used to characterize the percolation process of two-phase fracturing fluids in the matrix. The study area is divided into several bond cells, each with several virtual internal bonds. The connection of each bond in the bond cell is an abstract treatment of the permeability of the medium and does not represent the actual physical model of the micro-porosity, and the permeability of each bond cell is assumed by the virtual internal bonds, and the equation for controlling the seepage flow of each bond is[25]

$$k_b\frac{\partial^2 P_m}{\partial x^2}+Q_{int}=\frac{s_b}{\rho g}\cdot\frac{\partial P_m}{\partial t} \tag{1}$$

where k_b is the equivalent permeability coefficient; P_m is the matrix fluid pressure; Q_{int} is the source or sink; S_b is the equivalent water storage rate; ρ is the fluid density within the matrix; g is gravity; t is time.

In isotropic media, the equivalent permeability coefficient k_b, defined as the unit flow rate per unit hydraulic gradient, characterizes the ease with which a fluid can pass through an imaginary internal bond and is expressed as

$$k_b=\frac{K_m(V\pi)^{1/2}}{\mu\Omega} \tag{2}$$

where K_m is the matrix permeability; V is the bond cell volume, which is equivalent to the bond cell area in two-dimensional conditions; μ is the fluid viscosity; Ω is the total number of imaginary internal bonds in the bond cell. The equivalent water storage rate is given by S_b

$$S_b=\frac{S_m V}{\sum_{j=1}^{\Omega} l_j} \tag{3}$$

where S_m is the water storage rate of the substrate and the length of the jth imaginary internal bond.

2.2. Flow Model of Two-Phase Fracturing Fluid in Hydraulic Fracture. Based on the N−S equations, the interfacial tension term is introduced to study the flow velocity and pressure distribution of two-phase fracturing fluid in the fracture. As shown in Figure 2, since the width of the fracture is

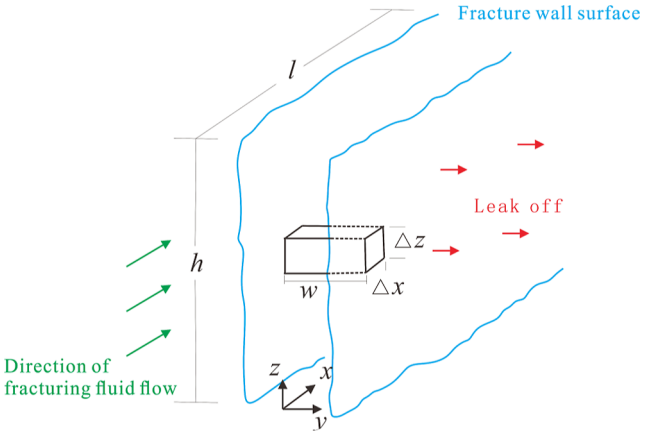

Figure 2. Physical model of two-phase fracturing fluid flow in a fracture.

much smaller than the fracture length and height, it can be approximated that two-phase fracturing fluid flows in two dimensions within the fracture, and its continuity equation is[26,27]

$$\frac{\partial(uw)}{\partial x}+\frac{\partial(vw)}{\partial z}+2v_{lm}=-\frac{\partial w}{\partial t} \tag{4}$$

where u and v are the flow rates in the x and z directions, m/s; w is the fracture width, m; v_m is the rate of leak-off.

According to the N−S equation, the rate of change of fluid momentum in a fluid cell in a fracture with time is equal to the combined force acting on the fluid in the cell,[28] and the two-phase fracturing fluid is considered as incompressible non-Newtonian fluid, whose momentum equation is

$$\begin{cases}-\dfrac{\partial P_f}{\partial x}+\left(\dfrac{\partial \tau_{xx}}{\partial x}+\dfrac{\partial \tau_{xz}}{\partial z}\right)+\rho f=0\\ -\dfrac{\partial P_f}{\partial z}+\left(\dfrac{\partial \tau_{zx}}{\partial x}+\dfrac{\partial \tau_{zz}}{\partial z}\right)+\rho(g+f)=0\end{cases} \tag{5}$$

where $\tau=\begin{pmatrix}\tau_{xx} & \tau_{xz}\\ \tau_{zx} & \tau_{zz}\end{pmatrix}=\mu\begin{pmatrix}2\dfrac{\partial u}{\partial x} & \dfrac{\partial u}{\partial z}+\dfrac{\partial v}{\partial x}\\ \dfrac{\partial v}{\partial z}+\dfrac{\partial u}{\partial x} & 2\dfrac{\partial v}{\partial z}\end{pmatrix}$; Pf is the fluid pressure within the fracture, which denotes continuous surface tension and reflects the effect of interfacial tension.

The continuous surface tension f can be calculated from the interfacial tension σ, and the volume fraction of PCL α is as follows[29]

$$f=-\sigma\left[\nabla\times\left(\frac{\nabla\alpha}{|\nabla\alpha|}\right)\right](\nabla\alpha) \tag{6}$$

where σ is the interfacial tension; α is the volume fraction of NPCL.

2.3. VOF Model Theory. In the field of computational fluid dynamics, the VOF method is used to study the interfacial distribution of two-phase fluids in the flow process, introducing a scalar function α that describes the ratio of the volume of one of the phases (PCL in this paper) in each cell to the volume of the cell itself. The fluid volume fraction is a dimensionless scalar function between 0 and 1. If its value is equal to 0, the control cell

https://doi.org/10.1021/acsomega.3c06877
ACS Omega 2024, 9, 2432−2442

contains only NPCL; if its value is equal to 1, the control cell contains only PCL; and if its value lies between 0 and 1, the control cell contains both PCL and NPCL.

In the VOF method, the two-phase fluid density ρ_0 and ρ_1 and two-phase viscosity μ_0 and μ_1 within the control cell during the two-phase flow are defined, and the density ρ and viscosity of the fluid ρ within the cell can be calculated by weighted averaging[29]

$$\rho = \alpha\rho_0 + (1-\alpha)\rho_1$$

$$\mu = \alpha\mu_0 + (1-\alpha)\mu_1 \tag{7}$$

where ρ_0 is the density of NPCL; ρ_1 is the density of PCL; μ_0 is the viscosity of NPCL; μ_1 is the viscosity of PCL.

The controlling equation for the volume fraction of fluid in the two-phase flow is

$$\frac{\partial\alpha}{\partial t} + \nabla\times(\alpha\vec{V}) = 0 \tag{8}$$

2.4. Initial and Boundary Conditions. In in situ-generated proppant fracturing, a high-viscosity conventional fracturing fluid is injected first to open the formation and form a hydraulic fracture, and then the two-phase fracturing fluid is injected. The initial moment when the two-phase fracturing fluid is injected is the initial moment, assuming a uniform distribution of fluid pressure within the fracture, and the initial pressure conditions are

$$P|_{T=0} = P_0 \tag{9}$$

Before the injection of two-phase fracturing fluid, no two-phase fracturing fluid was present in the fracture, so the initial volume fraction conditions were

$$\alpha|_{T=0} = 0 \tag{10}$$

The inflow boundary is the velocity boundary, the outflow boundary is the pressure boundary, and the fracture length is noted as L. The fracturing fluid has only velocity u_0 along the x-direction at the fracture mouth, the velocity v at the longitudinal upper boundary is 0, the distal end of the fracture is kept at the initial pressure P_0, and the PCL volume fraction at the injection end is a constant value α_0. Therefore, the boundary conditions can be written as

$$\begin{cases} u|_{x=0} = u_0 \\ v|_{x=0} = 0 \\ P|_{x=L} = P_0 \\ \alpha|_{x=0} = \alpha_0 \end{cases} \tag{11}$$

3. SOLUTION AND VALIDITY OF THE MODEL

3.1. Model Solution. For the two-phase fracturing fluid flow equation for the leak-off into the formation, the DVIB method is used to solve the equation. Treating each bond as a unit, the discrete form of eq 1 is

$$\boldsymbol{H}^b\boldsymbol{P}^b + \boldsymbol{S}^b\dot{\boldsymbol{P}}^b = \boldsymbol{Q}^b \tag{12}$$

where

$$\boldsymbol{H}^b = \frac{k_b}{l}\begin{bmatrix} 1 & -1 \\ -1 & 1 \end{bmatrix} \tag{13}$$

$$\boldsymbol{S}^b = \frac{s_b l}{\rho g}\begin{bmatrix} \frac{1}{3} & \frac{1}{6} \\ \frac{1}{6} & \frac{1}{3} \end{bmatrix} \tag{14}$$

$$\boldsymbol{Q}^b = \begin{bmatrix} q_i \\ q_j \end{bmatrix} \tag{15}$$

$$\boldsymbol{P}^b = \begin{bmatrix} p_i \\ p_j \end{bmatrix} \tag{16}$$

$$\dot{\boldsymbol{P}}^b = \begin{bmatrix} \dot{p}_i \\ \dot{p}_j \end{bmatrix} \tag{17}$$

The percolation equation can be assembled by using the matrix form of each bond cell and then further assembled to obtain the flow equations for the entire discrete domain

$$\boldsymbol{H}\boldsymbol{P} + \boldsymbol{S}\dot{\boldsymbol{P}} = \boldsymbol{Q} \tag{18}$$

For the two-phase fracturing fluid flow equation within the fracture shown in eq 5, the x-direction control equation within each integral grid cell Ω^e can be written as

$$\begin{aligned} &\left[2\mu\iint_{\Omega^e}\frac{\partial\Phi}{\partial x}\frac{\partial\Phi^T}{\partial x}\mathrm{d}x\mathrm{d}y + \mu\iint_{\Omega^e}\frac{\partial\Phi}{\partial y}\frac{\partial\Phi^T}{\partial y}\mathrm{d}x\mathrm{d}y\right]{u_I}^e \\ &\quad + \left[\mu\iint_{\Omega^e}\frac{\partial\Phi}{\partial x}\frac{\partial\Phi^T}{\partial x}\mathrm{d}x\mathrm{d}y\right]{v_I}^e - \left[\iint_{\Omega^e}\frac{\partial\Phi}{\partial x}\Phi^T\mathrm{d}x\mathrm{d}y\right]{p_I}^e \\ &\quad + \iint_{\Omega^e}\rho f\,\mathrm{d}x\mathrm{d}y \\ &= -\int_{\Gamma^e}\Phi\Phi^T{p_I}^e\cos\theta_x\mathrm{d}\Gamma \end{aligned} \tag{19}$$

where Φ is the interpolation function; v_I^e represents the velocity of each node in the cell; p_I^e is the pressure of each node in the cell; Γ is the boundary; and θ_x is the angle of the direction normal to the boundary outside. Equation 19 can be written in matrix form as

$${D_{11}}^e{u_I}^e + {D_{12}}^e{v_I}^e - C_1{p_I}^e + {E_1}^e = -{F_1}^e \tag{20}$$

Similarly, the momentum equation in the y-direction can be converted into matrix form

$${D_{21}}^e{u_I}^e + {D_{22}}^e{v_I}^e - C_2{p_I}^e + {E_2}^e = -{F_2}^e \tag{21}$$

The expressions for the coefficients in eqs 20 and 21 can be calculated by Gaussian integration.[30]

The equation for controlling the volume fraction of the fluid shown in eq 8 can be written as

$$\alpha_{\Omega_e}^{n+1} = \alpha_{\Omega_e}^{n} - \frac{1}{V}\sum_{s=1}^{NF}\alpha_s^n V_s^n A_s^n \Delta t \tag{22}$$

where $\alpha_{\Omega e}^{n+1}$ denotes the volume fraction within the cell at the moment $n+1$; $\alpha_{\Omega e}^{n}$ denotes the volume fraction Ω_e within the cell Ω_e at the moment n; α_s^n denotes the volume fraction of fluid at the surface s within the cell Ω_e at the moment n; V_s^n denotes the velocity vector at the surface s of the control body; A_s^n denotes the outer normal vector at the surface s of the control body.

https://doi.org/10.1021/acsomega.3c06877
ACS Omega 2024, 9, 2432−2442

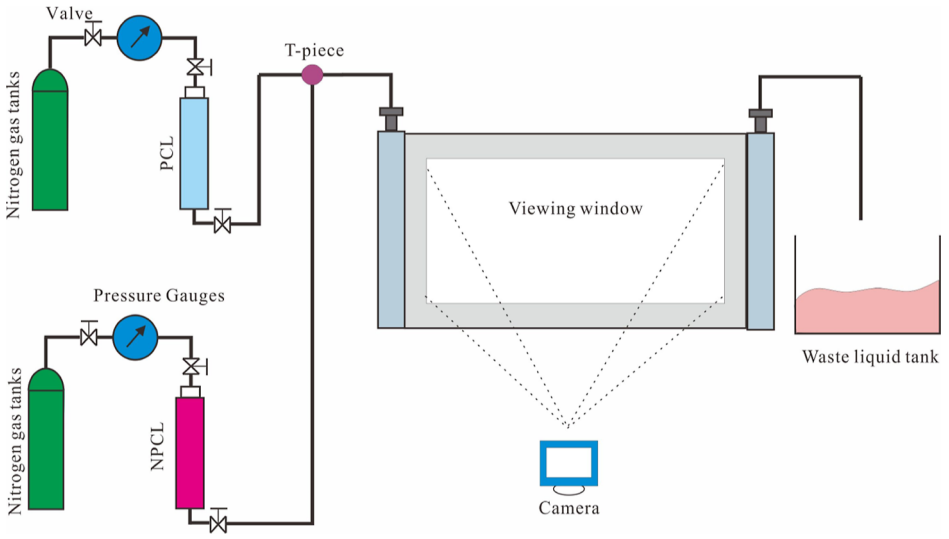

Figure 3. Liquid−liquid two-phase flow pattern distribution experimental setup.

Table 1. Main Experimental Parameters for Physical Experiments

experiment no	density, kg/m^3		interfacial tension, mN/m	viscosity, mPa·s		injected displacement, L/min	injection proportion, volume of NPCL VS volume of PCL
1	NPCL	1000	15	NPCL	10	4.73	3:1
2	PCL	1050		PCL	40		2:1
3							1:1

Figure 4. Flow patterns at different NPCL and PCL ratios as measured by physical experiments.

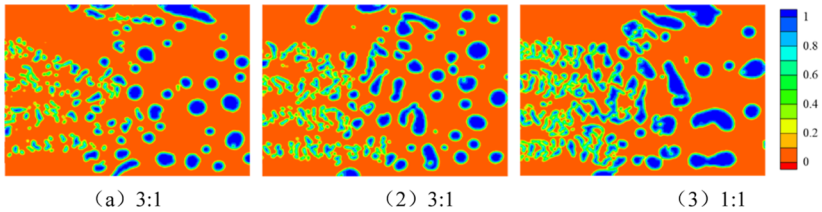

Figure 5. Numerical simulation results of flow patterns for different NPCL and PCL ratios.

3.2. Validity of the Model. The flow pattern distribution of PCL and NPCL under different experimental parameters was carried out by using the visualized liquid−liquid two-phase flow pattern distribution experimental apparatus, as shown in Figure 3, and the experimental results were used to verify the mathematical model established in this paper. The experimental parameters are shown in Table 1, and the experimental results under different PCL and NPCL ratio conditions are shown in Figure 4, where the light yellow liquid is PCL and the blue liquid is NPCL.

From the physical simulation experiments, the PCL is distributed in the form of a dispersed phase, showing droplet shape and striped shape distribution. When the ratio of NPCL to PCL is 3:1, it tends to form a round spherical distribution, and when the ratio of NPCL to PCL is 1:1, it tends to form a striped shape distribution. Based on the experimental data shown in Table 1, the flow distribution under different injection ratios was simulated using the established mathematical model, and the simulation results are shown in Figure 8.

The results of the numerical simulation of the flow pattern under different NPCL and PCL ratios are shown in Figure 5, where the color indicates the volume fraction of the PCL on the grid. The numerical simulation results shown in Figure 5 are close to the physical experimental results shown in Figure 4, where PCL is distributed in the form of dispersed phases, showing a droplet, striped distribution. When the ratio of NPCL to NPCL is 3:1, the volume of NPCL is high, and PCL is mainly distributed in the flow region in the form of droplet spheres. As the volume fraction of PCL increases, PCL tends to cluster together, resulting in a significant increase in PCL size. In the

https://doi.org/10.1021/acsomega.3c06877
ACS Omega 2024, 9, 2432−2442

physical experiment, there are several small orifices at the left inlet end, and the liquid enters through the small orifices into the visible range of the observation window; therefore, the PCL droplet size is smaller at the inlet end and gradually increases in size during the flow process, and a similar phenomenon can be observed in the results of the numerical simulation experiment shown in Figure 5.

4. CASE STUDY

The flow pattern of the two-phase fracturing fluid is greatly influenced by the injection displacement, interfacial tension, and the volume ratio of PCL and NPCL.

4.1. Influence of Injection Displacement on the Flow Pattern. PCL morphology and size were found to be strongly influenced by the shear rate in previous indoor experimental studies.[20,24] During Fracking field construction, the shear speed of the two-phase fracturing fluid in the fracture is different under different injection displacements, resulting in different PCL discrete phases and sizes. To investigate the effect of displacement on the morphology and size of PCL aggregates, the flow distribution patterns were calculated for different displacement rates of 3, 4, 5, and 6 m^3/min based on the calculated parameters shown in Table 2. The flow pattern distribution of PCL in the fracture at the end of the injection at different displacement volumes is shown in Figure 6.

Table 2. Main Parameters Used in Numerical Simulations

parameters	values	parameters	values
injected displacement, m^3/min	5	injection time, min	40
bottom hole pressure, MPa	43	reservoir pore pressure MPa	40
fracture length, m	100	fracture height, m	30
PCL density, kg/m^3	1050	NPCL density, kg/m^3	1000
interfacial tension, mN/m	25	PCL volume fraction	30%
PCL viscosity, mPa·s	40	NPCL viscosity, mPa·s	10

The higher the injection displacement, the higher the shear rate to which the two-phase fracturing fluid is subjected, and the more likely the PCL forms a droplet shape, while at lower injection displacement, the shear rate is lower, and the PCL is more likely to form a striped shape distribution. When the injection displacement is 3 and 4 m^3/min, the PCL in the whole fracture shows a striped shape distribution with a larger size, and the long axis of the striped shape PCL tends to face the direction of fluid flow. As the injection displacement rises to 5 m^3/min, the shear time is shorter near the injection end, again forming a striped PCL, and at approximately 60 m from the seam mouth, the shear time is longer, and the shear rate is sufficiently large to cause the PCL to form a distribution pattern close to that of a sphere. As the displacement continues to increase to 6 m^3/min, a rounded spherical flow pattern begins to form at approximately 50 m from the slit opening.

As shown in Figure 7, the PCL volume fraction values on six uniformly distributed cross sections were intercepted in the

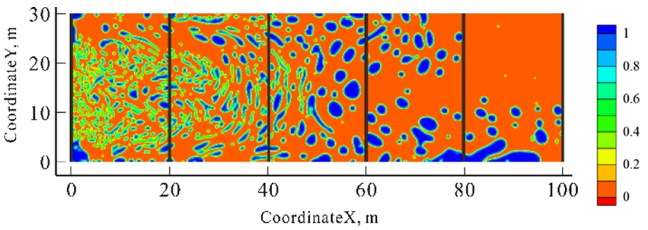

Figure 7. Schematic diagram of the position of the cutoff line.

fracture length direction, with the x-coordinates of the cross-section locations being 0, 20, 40, 60, 80, and 100 m. The PCL volume fraction values on the cross sections at different displacements are listed in Figure 8. Clearly, the number of wave peaks in each curve in the figure represents the number of PCL aggregates in the corresponding cross-section, and the peak of the wave represents the PCL volume fraction in the PCL aggregates. As the boundary condition given on the entrance boundary is the volume fraction of PCL, the shear time at the seam mouth is short, PCL has not yet aggregated under the action of interfacial tension, and PCL and NPCL are in a mixed-phase, intercalated state, so the volume fraction at the seam mouth position (i.e., at 0 m) is generally less than 1, and the number of wave peaks is high. In the direction away from the seam mouth, the number of wave peaks gradually decreases, while the peak value of the wave gradually approaches 1,

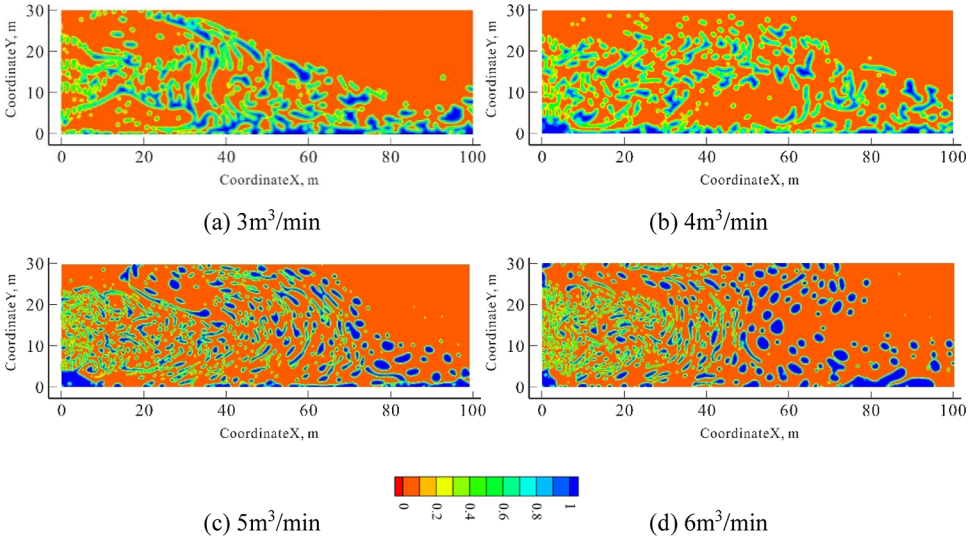

Figure 6. Flow pattern of two-phase fracturing fluid at different injection displacements.

https://doi.org/10.1021/acsomega.3c06877
ACS Omega 2024, 9, 2432−2442

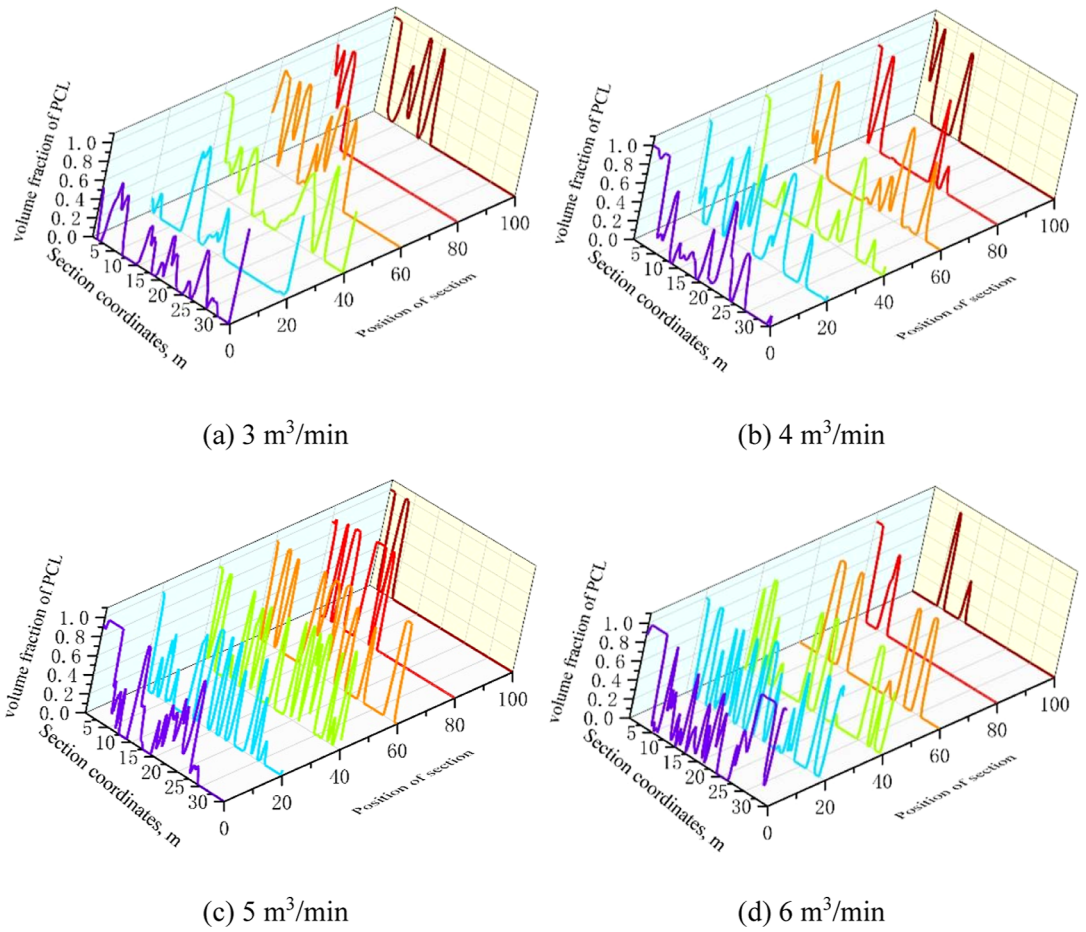

Figure 8. PCL volume fraction for different displacements and different cutoff positions.

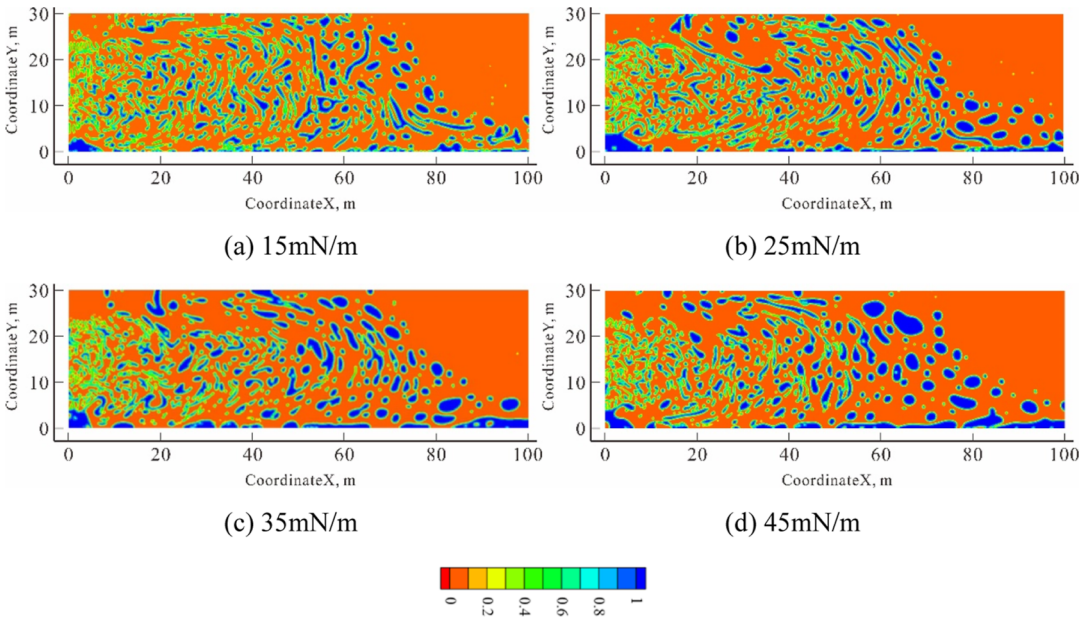

Figure 9. Flow pattern of the two-phase fracturing fluid at different interfacial tensions.

indicating that the number of PCL aggregates gradually decreases, and they gradually show a nonmiscible, nonmixed-phase state with NPCL under the action of interfacial tension. As the denser PCL tends to sink to the bottom under the action of gravity, the number of PCL aggregates decreases significantly in the cross sections at 80 and 100 m.

4.2. Influence of Interfacial Tension on the Flow Pattern. Two-phase fracturing fluid is a liquid−liquid two-phase system. Under the action of interfacial tension, the

https://doi.org/10.1021/acsomega.3c06877
ACS Omega 2024, 9, 2432−2442

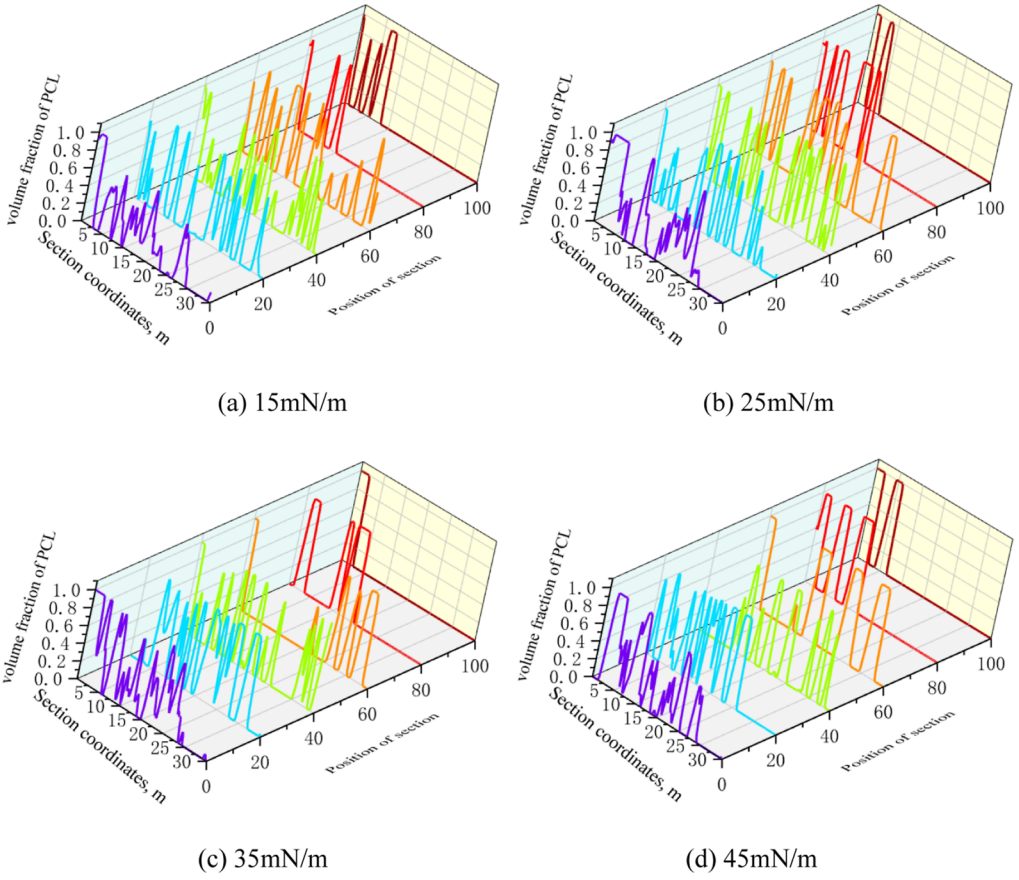

Figure 10. Volume fraction of PCL for different interfacial tensions and different truncation positions.

molecules on the surface layer of the two-phase fluid are subjected to the gravitational force of the internal molecules and tend to move toward the interior, i.e., there is a tendency to reduce the surface area of the fluid. The interfacial tension is perpendicular to the boundary of the surface and points to the interior of the fluid. Therefore, it is necessary to study the flow distribution morphology of the phase change in the fracturing fluid system under different interfacial tensions and analyze the mechanism of different flow pattern formations under the action of interfacial tensions. Based on the calculation parameters shown in Table 2, the flow distribution patterns were calculated for interfacial tensions of 15, 25, 35, and 45 mN/m, respectively, and the results are shown in Figure 9.

From the energy point of view, surface tension drives the surface of the liquid, which tends to be the lowest energy state; in the liquid surface layer of molecules, the thin, interfacial tension perpendicular to the surface boundary, pointing to the liquid inside, tends to contract so that the liquid as much as possible reduces its surface area; therefore, the smaller the size of PCL aggregates, its specific surface, that is, the total area per unit mass of liquid, the larger it is, the higher the energy. When the interfacial tension is small, the ability of PCL to contract is weak, forming a larger specific surface and a smaller liquid pearl size. When the interfacial tension is as low as 15 mN/m, it is difficult for PCL to contract under the impact of NPCL, showing a striped shape distribution instead of a droplet shape distribution. As the interfacial tension increases, the contraction ability of PCL increases, the size of the beads formed increases, and the specific surface area decreases. When the interfacial tension increases to 25 mN/m, it can form a droplet shape distribution at the distal end of the fracture, and when the interfacial tension increases to 35 and 45 mN/m, the contraction ability of PCL is further enhanced; PCL mainly exists in the form of droplets, and its size is larger than that at 25 mN/m.

The PCL volume fractions for different interfacial tensions and different truncation positions are shown in Figure 10. Similar to the results of PCL volume fraction under different displacements, the boundary condition given on the inlet boundary is the volume fraction of PCL, the shearing time at the seam mouth is short, PCL has not yet been aggregated under the action of interfacial tension, PCL and NPCL are in an immiscible state, the number of waves of PCL volume fraction curves under different truncation position conditions is high, and the PCL volume fraction at the seam mouth under different interfacial tensions is similar. After the distance in the fracture length direction exceeded 40 m, the PCL volume fraction at different interfacial tensions varied greatly, and the number of wave peaks at the same truncation positions and different interfacial tensions tended to decrease with increasing interfacial tensions.

4.3. Influence of PCL Volume Fraction on the Flow Pattern. The larger the PCL volume fraction, the more space it occupies, and different fluid distribution patterns will occur under different PCL volume fraction conditions. To investigate the formation mechanism of flow distribution patterns at different PCL volume fractions, the two-phase fracturing fluid flow distribution patterns were calculated at 10, 20, 30, and 40% PCL volume fractions on the injection boundary. The distribution pattern of two-phase fracturing fluid in the fracture zone at different volume fractions is shown in Figure 11.

https://doi.org/10.1021/acsomega.3c06877
ACS Omega 2024, 9, 2432−2442

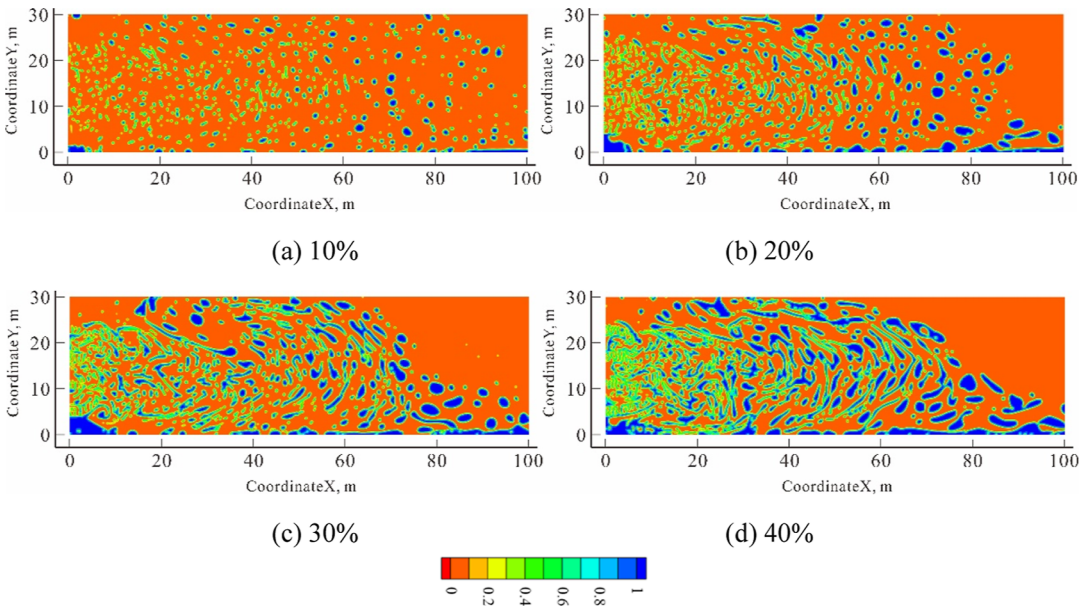

Figure 11. Flow pattern of two-phase fracturing fluid at different PCL volume fractions.

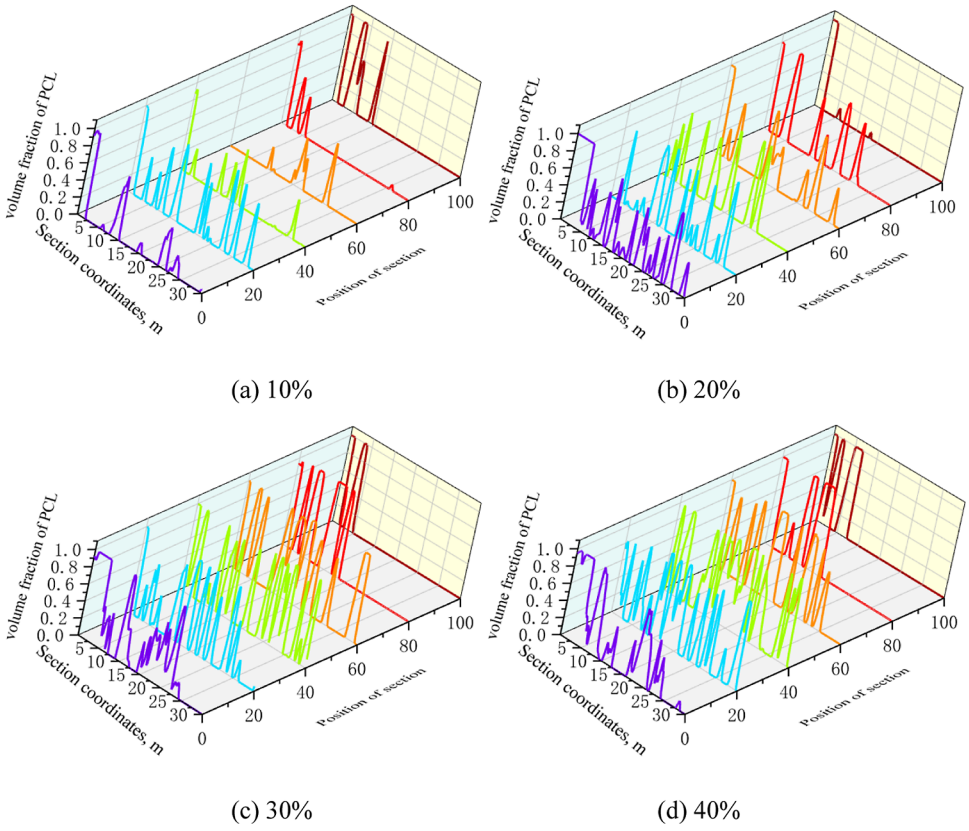

Figure 12. PCL volume fraction for different PCL ratios and different truncation positions.

At different volume fractions, the two-phase fracturing fluid shows different flow patterns. When the volume fraction of PCL is low (10%), PCL is distributed in a dispersed droplet shape within the fracture and tends to shrink together, but due to the low volume fraction of PCL, the droplets are relatively dispersed and occupy a small total area within the fracture, making it difficult to adequately support the artificial fracture. When the volume fraction of PCL is increased to 20%, when the volume fraction increases to 30 and 40%, the droplets of PCL tend to join together in the direction of the fracture length and show a striped shape distribution.

Figure 12 shows the PCL volume fractions for different PCL ratios and different truncation positions. When the PCL volume fraction is low (10%), the PCL is distributed in a sparse bead form within the fracture; therefore, the PCL volume fraction curve peaks at different truncation positions are less, and most of the peak values are less than 1, indicating that the PCL volume fraction is small and the PCL and NPCL may show mutual

https://doi.org/10.1021/acsomega.3c06877
ACS Omega 2024, 9, 2432−2442

solubility. The number gradually increases, and the peak value of the volume fraction curve at 60 and 80 m within the seam can reach 1, indicating that only PCL exists within the calculated grid. After the volume fraction of PCL increases to 30% and 40%, the number of curve peaks further increases and the width of the peaks increases, indicating that the size of the PCL aggregates formed is larger.

5. RESULTS AND DISCUSSION

5.1. Shape of the PCL. In a two-phase fluid system, the dispersed phase always tends to reach the lowest energy state under the action of interfacial tension, the surface area has a tendency to contract, thus making the liquid reduce its surface area as much as possible, and the sphere (round in two-dimensional conditions) is the geometry with the smallest surface area under a certain volume; therefore, under the combined action of interfacial tension and shear, the PCL aggregates always tend to be round.

5.2. Injection Parameter Optimization Design. The higher the injection displacement, the higher the shear rate to which the two-phase fracturing fluid is subjected, and the more likely the PCL forms a droplet shape, while at lower injection displacement, the shear rate is lower and the PCL is more likely to form a striped shape distribution. Therefore, to achieve a better prop effect, the displacement should be appropriately increased.

When the interfacial tension is small, it tends to form a larger specific surface and a smaller liquid pearl size. As the interfacial tension increases, the size of the beads formed increases, and the specific surface area decreases. Therefore, to increase the size of the IGP and the conductivity of the hydraulic fracture, the interfacial tension should be appropriately increased.

When the volume fraction of PCL is low, the PCL droplets are relatively dispersed and occupy a small total area within the fracture, making it difficult to adequately support the artificial fracture. However, the PCL may take up too much fracture space under a high volume fraction. When fracturing, the PCL ratio needs to be optimized to strike a balance between a good prop effect and high conductivity.

6. CONCLUSIONS

This paper, based on the physical properties of two-phase fracturing fluid and in situ-generated proppant fracturing technology, establishes a mathematical model of two-phase fracturing fluid flow distribution, using numerical experiments to analyze the two-phase flow pattern under different injection displacements, interfacial tensions, and PCL ratios, mainly obtaining the following conclusions:

(1) At lower injection displacement (3 or 4 m^3/min), it is easier to form a striped shape distribution, and at higher injection displacement (5 or 6 m^3/min), it is easier to form a droplet shape distribution. Therefore, when constructing on site, appropriately increasing the discharge volume helps to shorten the construction time, reduce the amount of leak-off, increase the shear rate, make the phase change fluid show liquid droplet shape distribution, and improve the injection capacity and support effect.

(2) Interfacial tension has a strong influence on the flow pattern, and its mechanism of action on the flow pattern is to control the degree of dispersion of the two-phase fluid. When the interfacial tension is small (15 mN/m), the contraction capacity of PCL is weak and distributed in strips; when the interfacial tension is large (23, 35, 45 mN/m), the contraction capacity of PCL increases and is mainly distributed in the form of droplets in the fracture.

(3) At lower volume fractions (10 and 20%), PCL tends to form discrete droplet shape distributions with poor support and possible fracture closure; at moderate volume fractions (30%), striped shape distributions begin to form; at higher volume fractions (40%), droplets of PCL come into contact with each other and occupy a large amount of space within the fracture, forming striped shape distribution patterns of larger size, resulting in oil and gas The flow channels are reduced. To achieve a better support effect and flow capacity, the volume fraction of PCL needs to be optimized to find a balance between effective support and high flow capacity channel construction

In summary, this paper focuses on the in situ-generated proppant fracturing technology that is solid-proppant-free to investigate the formation mechanisms of different flow patterns in a two-phase fracturing fluid, revealing flow pattern differences under different injection displacements, interfacial tensions, and PCL volume fractions, which enrich the theoretical system of in situ-generated proppant fracturing technology and can provide theoretical support for the on-site implementation of this technology.

AUTHOR INFORMATION

Corresponding Author

Yusong Chen − *CCDC Shale Gas Exploration and Development Department, Chengdu 610000, China;* orcid.org/0009-0000-6245-4620; Email: ychen20200910@163.com

Authors

Jingwei Li − *CCDC Shale Gas Exploration and Development Department, Chengdu 610000, China*

Qi Song − *Computing Center for Geotechnical Engineering, Zhejiang University, Zijingang, Hangzhou 310058, China; Research Center of Coastal and Urban Geotechnical Engineering, Zhejiang University, Zijingang, Hangzhou 310058, China*

Chengzhong Bu − *CCDC Shale Gas Exploration and Development Department, Chengdu 610000, China*

Kairui Ye − *CCDC Shale Gas Exploration and Development Department, Chengdu 610000, China*

Feng He − *CCDC Shale Gas Exploration and Development Department, Chengdu 610000, China*

Zhuolun Lv − *CCDC Shale Gas Exploration and Development Department, Chengdu 610000, China*

Xiang Chen − *School of Automation, Chengdu University of Information Technology, Chengdu 610500, China*

Complete contact information is available at: https://pubs.acs.org/10.1021/acsomega.3c06877

Notes

The authors declare no competing financial interest.

ACKNOWLEDGMENTS

This work was supported by the CCDC-Yangtze University cooperation project of unconventional oil and gas exploration and development, 2022 (CQCJ-2022-05).

https://doi.org/10.1021/acsomega.3c06877
ACS Omega 2024, 9, 2432−2442

REFERENCES

(1) Zhang, N.; Luo, Z.; Zhao, L.; Zhu, R.; Chen, W.; Liu, G.; Chen, X.; Xie, Y.; Cheng, L. Innovative thermo-responsive in-situ generated proppant: Laboratory tests and field application. *J. Pet. Sci. Eng.* **2022**, *208*, 109514.

(2) Zhang, N.; Luo, Z.; Chen, X.; Miao, W.; Xie, Y.; Cheng, L.; Yu, J.; He, J. Effect of the variation of phase-transition fracturing fluid thermophysical properties on the wellbore temperature. *Geoenergy Sci. Eng.* **2023**, *223*, 211587.

(3) Luo, Z. F.; Zhang, N. L.; Zhao, L. Q.; Pei, Y.; Liu, P.; Li, N. Thermoresponsive in Situ Generated Proppant Based on Liquid-Solid Transition of a Supramolecular Self-Propping Fracturing Fluid. *Energy Fuels* **2019**, *33* (11), 10659−10666.

(4) Zhang, N. L.; Chen, Z. X.; Luo, Z. F.; Liu, P.; Chen, W.; Liu, F. Effect of the phase-transition fluid reaction heat on wellbore temperature in self-propping phase-transition fracturing technology. *Energy* **2023**, *265*, 126136.

(5) Chen, X.; Zhao, L.; Liu, P.; Du, J.; Wang, Q.; An, Q.; Chang, B.; Luo, Z.; Zhang, N. Experimental study and field verification of fracturing technique using a thermo-responsive diverting agent. *J. Nat. Gas Sci. Eng.* **2021**, *92*, 103993.

(6) Yang, Z.; Wang, J.; Zhang, J.; He, L.; Luo, X.; Su, H.; He, X. A statistical method for flow pattern and efficiency prediction using pressure drop in a two-stage gas liquid cylindrical cyclone. *J. Nat. Gas Sci. Eng.* **2022**, *99*, 104414.

(7) Zhang, T.; Guo, K.; Liu, C.; Feng, A.; Cai, H.; Ren, S. Numerical simulation and experimental study of liquid-liquid flow dispersion in conical spiral pipes. *Chem. Eng. Res. Des.* **2018**, *138*, 374−386.

(8) Archibong-Eso, A.; Shi, J.; Baba, Y. D.; Aliyu, A. M.; Raji, Y. O.; Yeung, H. High viscous oil-water two-phase flow: experiments & numerical simulations. *Heat Mass Transfer* **2019**, *55* (3), 755−767.

(9) Abdul Hussein, H. M.; Ahmed, S. T.; Habeeb, L. J. Numerical and experimental investigation of two phase flow geometrical characteristics. *Curved Layer. Struct.* **2022**, *9* (1), 212−226.

(10) Song, Z.; Yang, L.; Hou, J.; et al. Characteristics of oil-water two-phase flow in the crack of fractured-vuggy reservoir. *J. Xi'an Shiyou Univ., Nat. Sci. Ed.* **2018**, *33* (04), 49−54.

(11) Babaoğlu, N. U.; Parvaz, F.; Hosseini, S. H.; Elsayed, K.; Ahmadi, G. Influence of the inlet cross-sectional shape on the performance of a multi-inlet gas cyclone. *Powder Technol.* **2021**, *384*, 82−99.

(12) Sarkar, P. S.; Singh, K. K.; Shenoy, K. T.; Sinha, A.; Rao, H.; Ghosh, S. K. Liquid-Liquid Two-Phase Flow Patterns in a Serpentine Microchannel. *Ind. Eng. Chem. Res.* **2012**, *51* (13), 5056−5066.

(13) Mao, G.; Xie, L.; Wang, K.; Li, Z. Flow pattern analysis of the oil-water batch transportation using a wheel flow loop. *Geoenergy Sci. Eng.* **2023**, *223*, 211534.

(14) Tan, J.; Jing, J.; Hu, H.; You, X. Experimental study of the factors affecting the flow pattern transition in horizontal oil-water flow. *Exp. Therm. Fluid Sci.* **2018**, *98*, 534−545.

(15) Wang, Y.; Yang, J.; Wang, T.; Hu, Q.; Lv, Z.; He, T. Visualization experiment of multi-stage alternating injection acid fracturing. *Energy Rep.* **2022**, *8*, 9094−9103.

(16) Zhang, N.; Luo, Z.; Chen, Z.; Liu, F.; Liu, P.; Chen, W.; Wu, L.; Zhao, L. Thermal−hydraulic−mechanical−chemical coupled processes and their numerical simulation: a comprehensive review. *Acta Geotech.* **2023**, *18*, 6253−6274.

(17) Leung, C. T. O.; Zimmerman, R. W. Estimating the Hydraulic Conductivity of Two-Dimensional Fracture Networks Using Network Geometric Properties. *Transp. Porous Media* **2012**, *93* (3), 777−797.

(18) Welch, N. J.; Carey, J. W.; Frash, L. P.; Hyman, J. D.; Hicks, W.; Meng, M.; Li, W.; Menefee, A. H. Effect of Shear Displacement and Stress Changes on Fracture Hydraulic Aperture and Flow Anisotropy. *Transp. Porous Media* **2022**, *141* (1), 17−47.

(19) Zhao, L.; Zhang, N.; Zhang, Y.; et al. Laboratory study and field application of self-propping phase-transition fracturing technology. *Nat. Gas Ind.* **2020**, *40* (11), 60−67.

(20) Zhao, L.; Chen, Y.; Du, J.; Liu, P.; Li, N.; Luo, Z.; Zhang, C.; Huang, F. Experimental Study on a new type of self-propping fracturing technology. *Energy* **2019**, *183*, 249−261.

(21) Economides, M. J.; Mikhailov, D. N.; Nikolaevskiy, V. N. On the problem of fluid leakoff during hydraulic fracturing. *Transp. Porous Media* **2007**, *67* (3), 487−499.

(22) Wang, F.; Pan, Z.; Zhang, S. Modeling Water Leak-off Behavior in Hydraulically Fractured Gas Shale under Multi-mechanism Dominated Conditions. *Transp. Porous Media* **2017**, *118* (2), 177−200.

(23) Xianwu, X.; Zheng, L. A discussion on the methods of calculating filtration coefficient of fracturing fluid in coal bed. *Nat. Gas Ind.* **2001**, *21* (3), 45−46.

(24) Chen, Y.; Sang, Y.; Guo, J.; Yang, J.; Chen, W.; Zeng, J.; Tang, B.; He, T. Experimental Study on a Liquid-Solid Phase-Change Autogenous Proppant Fracturing Fluid System. *ACS Omega* **2023**, *8* (10), 9101−9110.

(25) Peng, S. J.; Zhang, Z. N.; Li, C. F.; He, G.; Miao, G. Simulation of water flow in fractured porous medium by using discretized virtual internal bond. *J. Hydrol.* **2017**, *555*, 851−868.

(26) Dong, C.; Zhu, D.; Hill, A. D. Modeling of the Acidizing Process in Naturally Fractured Carbonates. *SPE J.* **2002**, *7* (04), 400−408.

(27) Mou, J.; Zhang, S. Modeling acid leakoff during multistage alternate injection of pad and acid in acid fracturing. *J. Nat. Gas Sci. Eng.* **2015**, *26*, 1161−1173.

(28) Yan, Z.; Zhu, X.; Wang, P.; Li, X.; Yu, S.; Li, Y.; Xue, Q. The effect of gas injection velocity and pore morphology on displacement mechanisms in porous media based on CFD approach. *J. Nat. Gas Sci. Eng.* **2022**, *101*, 104558.

(29) Pei, Y.; Zhang, N.; Zhou, H.; Zhang, S.; Zhang, W.; Zhang, J. Simulation of multiphase flow pattern, effective distance and filling ratio in hydraulic fracture. *J. Pet. Explor. Prod. Technol.* **2020**, *10* (3), 933−942.

(30) Bi, C. *Finite element method of computational fluid dynamics and its programming*; China Machine Press, 2013.

https://doi.org/10.1021/acsomega.3c06877
ACS Omega 2024, 9, 2432−2442